UAV Trajectory Optimization for Air-to-Water Optical Wireless Channels

Sk Samiul Reza[1] and Murat Yuksel[1],
[1]*University of Central Florida, Orlando, FL, USA*
sksamiul.reza@ucf.edu, murat.yuksel@ucf.edu

***Abstract*—The field of underwater optical wireless communication (UOWC) has garnered significant attention due to its potential applications in global climate monitoring, military operations, and marine biology research. UOWC offers several advantages, including higher transmission data rates and increased bandwidth utilization in unlicensed spectrum bands. However, it also faces challenges such as absorption, scattering, and turbulence, especially when dealing with the air-to-water (A2W) interface, which can be random and disruptive. This study involves simulation works that demonstrate how a dynamic water surface disrupts the communication channel between air and water in terms of received signal intensity. To address this issue, we explore the feasibility and advantages of optimizing the movements of the UAV optical transmitter to counteract the disruption caused by water surface waves. By simulating three optimized UAV movement strategies customized for value, reliability, and performance, across both intermediate and deep water scenarios, the study demonstrates their effectiveness in achieving improved communication, even in the presence of a disruptive water surface.**

***Index Terms*—Free-Space Optics, Air-Water Interface, Optical Wireless Communication, Underwater Optical Wireless Communication, Optical Beam Propagation, UAV Trajectory Optimization.**

I. Introduction

In the past twenty years, there has been a significant increase in interest in underwater wireless communication. This has been driven by various factors, including advances in oceanic exploration, focus on global warming, and the need for direct communication between submerged objects (such as submarines) and free-space equipment (like ships or communication satellites). The rapid advancement of unmanned aerial vehicles (UAVs) and autonomous underwater vehicles (AUVs) emphasizes the critical requirement for a stable telecommunications infrastructure to enable smooth data transfer between these platforms. While radio waves are effective in free space, they are ineffective underwater, limiting communication distance to only a few decimeters [1]. As a result, state-of-the-art underwater wireless communication techniques use sound waves to increase communication range. However, this method is vulnerable to eavesdropping and is only effective within a narrow frequency range of a few hundred KHz [2].

When a signal has to travel from air to water (A2W) or water to air (W2A), it experiences significant absorption and attenuation. Additionally, underwater environments are naturally noisy in the acoustic frequencies, with ambient noise coming from marine life, human activity, and natural surroundings. These noises can affect acoustic signals, reducing their reliability and clarity. Current acoustic-based solutions involve a floating platform (such as a buoy) at the water's surface, which acts as a communication relay between the free-space radio frequency (RF) signal and the underwater acoustic signal. However, this design is limited by the few hundred KHz bandwidth of the acoustic signals and location disclosure, making it unattractive for military applications that require a secure and covert communication channel.

Optical wireless communication (OWC) is an emerging technology that uses light to enable high-bandwidth communication between air and water. It offers minimal latency, low power consumption, and a wide communication range. This innovative approach allows for direct communication between submerged receivers and free-space transmitters [3]. However, its success depends on the designer's ability to assess signal attenuation and misalignment caused by unpredictable water waves at the air-water interface.

There is a significant research gap in understanding the impact of random water surfaces on the received intensity underwater, as well as how an airborne transmitter can optimize its movements to enhance communication with the submerged receiver. This paper aims to comprehensively address both aspects as:

- we demonstrate the influence of random water surface dynamics on the received intensity underwater.
- we define the optimization of the UAV's trajectory based on changing water surfaces, while considering UAV transmission to a submerged receiver through an OWC channel.
- we develop heuristic solutions for optimizing UAV trajectories, considering two water depths and emphasizing value, reliability, and performance.

The subsequent sections of the paper are organized as follows: section II discusses related research works. Section III outlines the system model, encompassing the calculation of received intensity for a single optical ray through a random water surface. Section IV presents simulation results for various UAV positions, correlating with the received intensity under varied horizontal and vertical movements of the water surface. Section V formulates three distinct UAV movement optimization problems, emphasizing value, reliability, and performance.

This work is supported in part by NSF award 2115215.

Section VI includes simulation results and a discussion on the optimization of UAV movement. Finally, section VII concludes our work.

II. Related Work

In the past decade, there has been significant interest in underwater optical wireless communication (UOWC) owing to its high data rates surpassing the Gbps boundary [4]. Numerous experimental studies have supported the theoretical findings as well [5]. The majority of studies on UOWC have delved into models related to underwater light scattering, absorption, and scintillation [6]. These investigations have focused on understanding the impact of these phenomena on underwater communications [7]. Additionally, researchers have explored the optimal wavelengths for UOWC systems in different water environments. Some initiatives have gone further to experimentally demonstrate higher data rate communication in UOWC. For instance, there have been efforts to achieve Gbps data rates using laser transmitters over short link ranges, employing light-emitting diode (LED) transmitters with a wavelength of 532 nm [8].

However, literature is scarce regarding communication between airborne and underwater nodes. The utilization of laser beams has been explored for creating an optical or opto-acoustic link [9]. However, the susceptibility of laser beams to errors in angular displacement becomes particularly pronounced when the airborne node is situated far from the surface. In addition to that, the randomness of the air-water surface poses a lot of challenges while establishing a cross-medium communication, in both directions [10]. In addressing signal distortions arising from the unpredictable air-water interface, [11] has introduced an adaptive optics system. This system relies on the understanding of wavefront distortions and adjusts the spatial phase to counteract optical aberrations and mitigate the impact of such distortions. However, such a system is quite expensive and complicated.

Researchers have also employed opto-acoustic energy transfer for communication across the air-water interface. In some cases, it focuses on the opto-acoustic downlink, employing a modulated laser beam directed at the water surface, with interception and demodulation of the corresponding underwater acoustic signal [12]. Conversely, [13] aims to validate the feasibility of opto-acoustic underwater communication and evaluate the bit error rate. However, the utilization of opto-acoustic conversion involves a complex process, necessitating the analysis of two distinct waves. Furthermore, the bandwidth is constrained by the underwater acoustic channel, which is considerably narrower than optical channels. To enable communication across medium boundaries, a new communication technology called translational acoustic-RF communication (TARF) is introduced to enable direct wireless communication between submerged underwater nodes and airborne nodes by transmitting acoustic signals and decoding them using an airborne mmWave radar. TARF achieves standard underwater bit rates up to 400 bps and can operate effectively in the presence of surface waves with amplitudes up to 16 cm peak-to-peak [14].

A2W optical wireless communication presents numerous advantages, positioning it as a promising technology for particular applications. Among these benefits are high data rates, low latency, and heightened security. Additionally, ongoing endeavors are in progress to address specific limitations associated with different aspects of the communication channel. Statistical models, incorporating the Birnbaum-Saunders distribution, are utilized to scrutinize the fading coefficient of AWOWC channels and the photon counting dynamics of single photon avalanche diode (SPAD). Analytical formulations for the bit error rate are derived to evaluate the performance of the communication link [15]. Research efforts have been dedicated to evaluating the bit error rate (BER) of L-ary pulse position modulation (L-PPM) over the sea surface under varying L values. The objective is to identify an optimal modulation method to effectively enhance the BER in the air-to-water communication channel [16].

Our study's key difference from the prior work is its detailed modeling of the impact of the water's surface randomness on the signal intensity of the AWOWC signal. Moreover, we employ movement optimization strategies to effectively address and mitigate these disruptive effects to attain seamless communication.

III. System Model

A. Assumptions and Limitations

We assume that there is a UAV hovering above the water surface which is offset around the x axis. The UAV hovers within coordinates: (30, 30), (30, 40), (40, 40), and (40, 30). Equipped with an optical wireless transmitter, the UAV utilizes a 530 nm laser with a fixed transmit power of 1 Watt and a beam angle of 20 degrees. The receiver, such as a photodetector, spans a width of 2 meters and is positioned from coordinates (34, -40) to (36, -40). It is attached to an AUV located 40 meters underwater and capable of detecting light intensity. The water is modeled to represent both deep (1000 m) and intermediate depths (250 m), with an attenuation coefficient of 0.151 m^{-1}, applicable for clear ocean water [17].

The transmitter on the UAV is not steerable, but the UAV can adjust its position to improve the light intensity at the receiver underwater. The transmitter is assumed to point perpendicular to the water surface level. Additionally, the UAV is assumed to have knowledge of the receiver's location and the capability to sense the shape of the water's surface waves. This capability can be achieved, for example, by inspecting reflections of periodically sent millimeter-wave sensory signals [14].

When calculating the channel behavior, as shown in Equation 4, we assume that only distance and beam angle contribute to the free-space loss. The transmitter emits 100 optical rays downward within the aperture of its beam angle. So, 100

equidistant optical rays are each 0.2 degrees apart from their adjacent rays.

We have assumed 21 sequential time instances during which the water surface wave moves horizontally from left to right, disrupting the wireless channel. For each period, specific to that particular water surface, $10 \times 10 = 100$ different UAV positions are considered. Each position is associated with a numeric value representing the summation of intensity captured by the underwater receiver for that specific position.

It is noteworthy that, for this work, we are only considering two-dimensional (2D) optical ray propagation for the transmitter and 2D movement optimization for the UAV. Three-dimensional (3D) water wave simulation, based on Stokes' Wave Theory, would require rigorous numerical methods such as the finite difference or the finite element method.

B. Water Surface Waves

The water surface is typically uneven due to wind and underwater currents. Therefore, precisely defining the equation for these surface waves is challenging. Figure 1 illustrates varied water surfaces with different heights and movements. In this depiction, the surface elevation follows a cnoidal function. As we can see, a cnoidal wave features a more pronounced crest and a flatter trough compared to a sine wave. In shallow water, the water wavelength is larger than the water depth (i.e., $\lambda > h$, where h is the water depth and λ is the wavelength of the water surface) and it is difficult to model the surface waves for shallow depths. We do not consider shallow waters and use the well-established Stokes' wave models [18] which apply to intermediate and deep water conditions. Deep water is defined by a water depth significantly greater than the wavelength: $h >> \lambda$. Following Stokes' third-order theory [18], the expression for water surface elevation can be articulated as follows:

$$\eta(x,t) = a\left[1 - \frac{1}{16}(k\cdot a)^2\cos\theta + \frac{1}{2}(k\cdot a)\cos 2\theta + \frac{3}{8}(k\cdot a)^2\cos 3\theta\right] \tag{1}$$

$$\theta(x,t) = kx - \omega t \tag{2}$$

$$k = \frac{2\pi}{\lambda}, \omega = 2\pi f, f = \frac{v}{\lambda} \tag{3}$$

Where $\eta(x,t)$ is the free surface height of the wave, which is a function of horizontal coordinates, x, and time, t. a is the first-order wave amplitude and k is the wave number. The wave phase is denoted as $\theta(x,t)$. Additionally, ω is the angular frequency, λ is the wavelength, and v is the phase velocity of the water surface wave. So, varying different parameters of Stoke's equation, for instance, the first-order wave amplitude a gives us wave shapes with different free water surface heights, resulting in the waves shifting vertically in the same period, whereas in the case of varying t, we could simulate water waves shifting horizontally with time as shown in Figure 1.

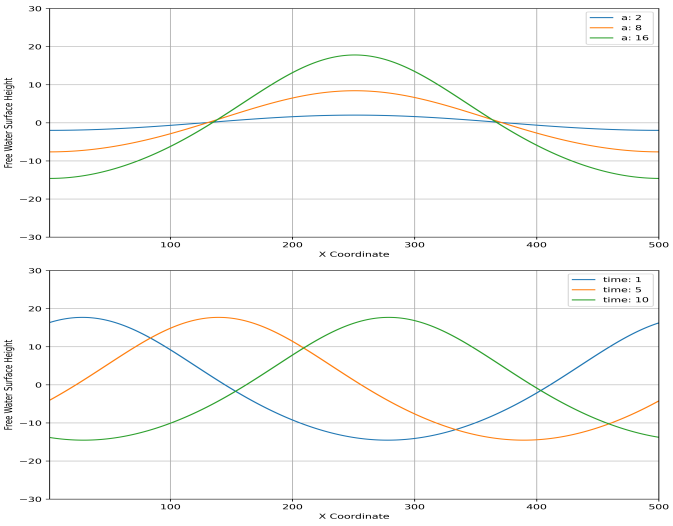

Fig. 1. Varied Water Surfaces for Different First-Order Wave Amplitudes (a) and Time.

C. Channel Model

1) Received Intensity from a Single Ray: An optical signal transmitted from the air goes through three stages of loss before reaching an underwater receiver:

1) free-space transmission loss,
2) air-to-water transmittance loss, and
3) underwater transmission loss.

An optical signal with power P milliwatts, that travels a distance of d_a meter in free-space, when the source beam angle is θ degree, the resultant intensity, I_a, in milliwatts per square meter would be [19]:

$$I_a = \frac{360}{\theta}\cdot\frac{P}{4\pi d_a^2}. \tag{4}$$

Assuming I_a is the intensity just above the water surface and from here on, the signal undergoes the loss associated with the air-water interface, which can be quantified via transmittance, τ. In that case, the intensity of the signal right below the water surface, I_w would be:

$$I_w = \tau \cdot I_a. \tag{5}$$

Then, the signal with intensity I_w travels through the water for a distance of d_w. Received intensity will depend on the attenuation coefficient of the water, $k(\lambda)$. Hence the intensity at the receiver, I_r, would be [20]:

$$I_r = I_w \cdot e^{-k(\lambda)d_w}. \tag{6}$$

By combining the three stages of attenuation, we get the end-to-end intensity equation, which is:

$$I_r = \frac{360}{\theta}\cdot\frac{P}{4\pi d_a^2}\cdot\tau\cdot e^{-k(\lambda)d_w}. \tag{7}$$

P and θ are dependent on the choice of the transmitter device, while $k(\lambda)$ depends on the water characteristics. For this work,

we have assumed these parameters to be constant. Hence, the received intensity for the A2W channel will eventually come down to:

$$I_r \propto \frac{\tau}{d_a^2 \cdot e^{d_w}}. \tag{8}$$

Next, we will discuss the process of determining transmittance (τ), air distance (d_a), and water distance (d_w) for a varied water surface.

2) Transmittance: For a cross-medium transmission, the signal that does not get transmitted is reflected to the originating medium. For optical wireless signals, when we have transmittance (τ) and reflectance (η), the relation between them is:

$$\tau = 1 - \eta. \tag{9}$$

In this work, we will consider an equal mixture of s and p polarized light. The difference between them is that the electric field vector in s-polarization is perpendicular to the incidence plane but parallel in the case of p-polarization [21]. Thus, the reflectance (η) would be:

$$\eta = \frac{\eta_s + \eta_p}{2}. \tag{10}$$

To calculate η_s and η_p, we need to use the Fresnel equation [22]. Assuming refractive indices of air and water are n_a and n_w, and the incident and refracted angles of the optical ray are θ_i and ϕ_r, we get:

$$\eta_s = \left| \frac{n_a \cos(\theta_i) - n_w \cos(\phi_r)}{n_a \cos(\theta_i) + n_w \cos(\phi_r)} \right|^2 \text{ and} \tag{11}$$

$$\eta_p = \left| \frac{n_a \cos(\phi_r) - n_w \cos(\theta_i)}{n_a \cos(\phi_r) + n_w \cos(\theta_i)} \right|^2. \tag{12}$$

3) Distance in Air and Water: To calculate the distance in air, it is sufficient to know the transmitter location and incident point location on the water surface. However, to determine the coverage area (on the water surface) for a single source, we need to take the source beam angle (θ) into consideration. For a source situated at y_t meters height in the air from a flat water surface offset at $y = 0$, the diameter of the coverage area (d_c) would be:

$$d_c = 2 \cdot y_t \cdot \tan\left(\frac{\theta}{2}\right). \tag{13}$$

However, the water surface is not always flat. As depicted in Figure 2, to get the leftmost and rightmost incident points for the transmitter, we need to find the intersection between the wide-most optical rays (shown in green) and the water surface curve (shown in blue). For example, for the left-most ray, a line equation needs to be formed through the coordinates $(x_t - \frac{d_c}{2}, 0)$ and (x_t, y_t). After that, it's just solving that line equation with the water surface Equation 1 to get the incident points. As shown in Figure 2, the incident rays from the transmitter at (x_t, y_t) would cover an area where the length d_c starts from the leftmost incident point to the rightmost one.

All the optical rays emitted from the transmitter lie within this length. Assuming the rays are equidistant, by putting the x coordinates from the coverage area in Equation 1, we will get all the incident points' coordinates, consequently getting the distance in the air (d_a). To calculate the underwater distance

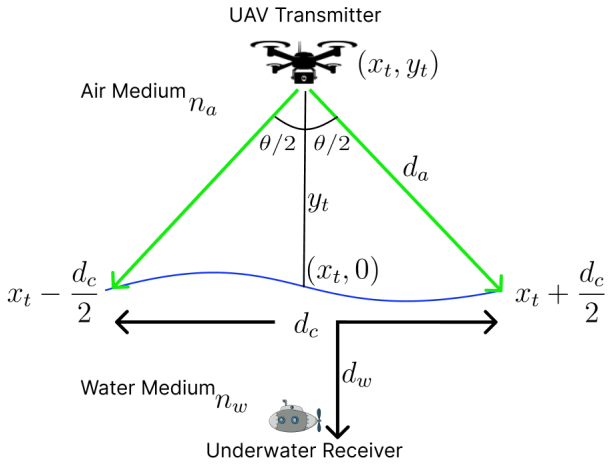

Fig. 2. Beam Coverage Calculation for UAV Transmitter.

(d_w), we need to consider the refraction as it changes the direction of the incident light, thus changing the incident point at the receiver plane underwater. Given that we already know the incident point on the water surface, if we can determine the incident point of the refracted optical ray at the underwater receiver plane, calculating the distance between two points will give our desired underwater distance (d_w). First, we will use Snell's Law [23] to establish the relation between incident angle and refracted angle:

$$n_a \sin(\theta_i) = n_w \sin(\phi_r). \tag{14}$$

As shown in Figure 3, to get the incident angle, we need the tangent and normal plane of the water surface at that incident point. To get the normal angle, first, we will have to differentiate Equation 1 with respect to x and substitute the x coordinate from the incident point to get the tangent angle (α):

$$\alpha = \frac{d}{dx}(\eta(x,t)). \tag{15}$$

Now, the relation between the normal angle (β) and the tangent angle (α) is:

$$\beta = \alpha + 90. \tag{16}$$

The normal angle (β) we get here is always with respect to the positive x-axis, so if we get the incident ray angle in a similar way, the difference would be the incident angle. As shown in Figure 4, assuming the incident point is (x_i, y_i) and transmitter coordinate is (x_t, y_t), the incident ray angle with positive x-axis (θ_{ir}) would be:

$$\theta_i r = \begin{cases} \theta_{ir}^p + 180°, & \theta_{ir}^p < 0°. \\ 90°, & x_i = x_t. \\ \theta_{ir}^p, & \theta_{ir}^p > 0°. \end{cases}$$

Where,

$$\theta_{ir}^p = \arctan\left(\frac{x_t - x_i}{y_t - y_i}\right). \tag{17}$$

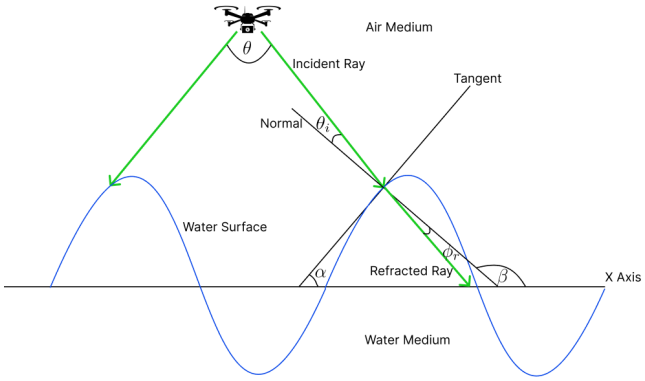

Fig. 3. Optical Ray Propagation from Air to Underwater.

Finally, the incident angle (θ_i), would be the difference between the normal angle (β) and the incident ray angle with positive x-axis (θ_{ir}):

$$\theta_i = |\beta - \theta_{ir}|\,. \tag{18}$$

Assuming we know the position of the receiver underwater, by calculating the refractive ray direction from the refractive angle, we can determine whether a particular optical ray will hit the receiver or not. Now refracted ray angle (ϕ_{rr}) can be determined like this:

$$\phi_{rr} = \begin{cases} \beta + 180° + \phi_r, & \theta_{ir} > \beta. \\ \beta + 180° - \phi_r, & \theta_{ir} < \beta. \\ \beta + 180°, & \theta_{ir} = \beta. \end{cases}$$

Also, the slope of the refracted ray (m_{rr}) is:

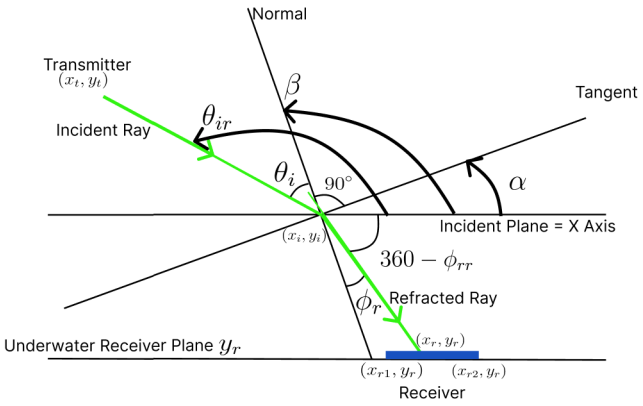

Fig. 4. Associated Angles in Optical Ray Refraction.

$$m_{rr} = \tan(\phi_{rr}) \tag{19}$$

As we already know the receiver's aperture from coordinate (x_{r1}, y_r) to (x_{r2}, y_r) on the plane y_r, we can easily determine whether the refracted optical ray will hit the receiver or not. Figure 4 shows the relationship between various angles during the refraction through the air-water interface. If (x_r, y_r) is the coordinate where the refracted ray will hit the receiver plane y_r, we can determine x_r like this:

$$x_r = \left(\frac{y_r - y_i}{m_{rr}}\right) + x_i, \tag{20}$$

where (x_i, y_i) is the incident point on the water surface. Now, if x_r lies in between x_{r1} and x_{r2}, that would be a successful transmission, and it will be added to the overall intensity with respect to that certain position (x_t, y_t) of the transmitter in the air.

4) Total Received Intensity: Assuming an optical transmitter in the air transmits N optical rays within its beam angle towards its incidental coverage area on the water surface, the total intensity is given by:

$$I_{\text{total}} = \sum_{r=1}^{N} I_r \cdot \chi_r. \tag{21}$$

Where I_r is the received intensity of the optical ray and χ_r is the indicator function (value 1 or 0) for whether the optical ray reaches the receiver aperture area or not.

TABLE I
SIMULATION PARAMETERS

Parameter	Symbol	Value (Intermediate, Deep Water)
Refractive Index of Air	n_a	1.0003 [19]
Refractive Index of Water	n_w	1.333 [19]
Attenuation Coefficient of Clear Ocean Water	$k(\lambda)$	0.151 m^{-1} [6]
Transmitter Beam Angle	θ	20 degrees
Transmit Power	P	1 W
Number of Time Instance	n	21
Wave Steepness	ka	0.3, 0.2 [24]
Water Wavelength	λ	500 m, 600 m [24]
Water Depth	h	250 m, 1000 m
*Wave Number	k	0.0125, 0.0105
**Phase Speed of the Water Wave	v	27.89 m/s, 30.61 m/s
**Water Wave Frequency	f	0.056 Hz, 0.051 Hz
**Angular Frequency	ω	0.350 rad/s, 0.321 rad/s

* Calculated based on λ.
** Calculated based on k and h.

IV. Effect of Random Water Surface on The Communication Channel

In this section, we will observe the effect of varied water surfaces on the optical wireless channel between air and underwater, and demonstrate the necessity for UAV movement optimization to mitigate this disruption. The water surfaces will be varied by two parameters: changing the first-order wave amplitude, a, to increase the height of the wave, and by changing time, t, to move the waves horizontally. For every UAV transmitter position in the air, there will be a respective total received intensity at the underwater receiver. This means that if the UAV stays at that position in the air, it will be able to provide that amount of intensity to the underwater receiver. When the water surface is varied, it will impact this position-wise intensity. The assumptions for this simulation are the same as in Section III-A and Table I shows the rest of the parameters.

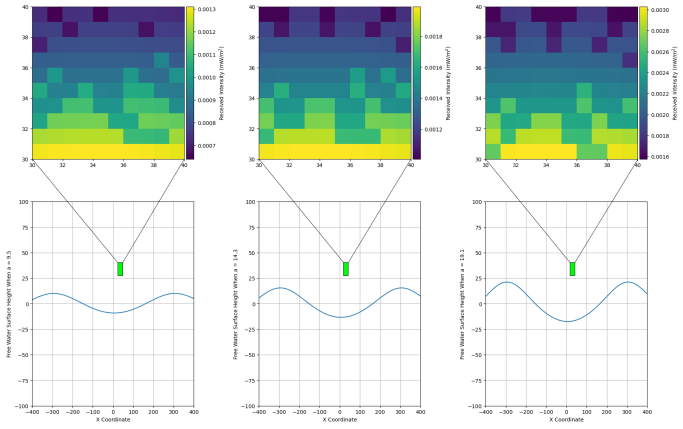

Fig. 5. Intensity Heatmap for Different Water Wave Amplitudes.

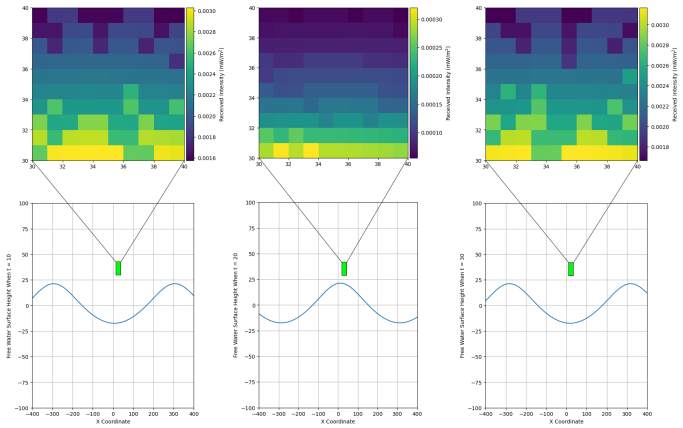

Fig. 6. Intensity Heatmap for Different Water Wave Horizontal Positions.

Figures 5 and 6 show the UAV heatmaps for the received intensity at the underwater receiver as, respectively, the amplitude and the horizontal position of the water wave change. The heatmaps clearly show that the random nature of the water surface has a significant impact on the communication in terms of received intensity, as in every scenario, the UAV positions that facilitate the high intensity at the receiver are different.

V. UAV Trajectory Optimization

We have shown that disruptive water waves create communication stability issues in A2W communication. Hence, instead of having the UAV hover at the same position, there is a scope for optimizing the UAV's trajectory as the water surface moves.

A. Problem Formulation

We consider the UAV trajectory optimization over n time intervals. Let $I_r(t)$ be the received light intensity at time interval $t \in \{1, .., n\}$, and Δt be the duration of a time interval in seconds. We can formulate the problem of maximizing the received light intensity over all time intervals as follows:

MTRI : Maximum Total Received Intensity

$$\max_{\hat{\boldsymbol{\epsilon}}} \sum_{t=1}^{n} I_r(t) \tag{22}$$

such that

$$P \leq P_{max}, \text{ and} \tag{23}$$

$$\frac{|\epsilon(t+1) - \epsilon(t)|}{\Delta t} \leq v_{max}, \quad t \in \{1, .., n-1\}, \tag{24}$$

where $\hat{\boldsymbol{\epsilon}} = \{\epsilon(1), .., \epsilon(n)\}$ are the positions of the UAV over n time intervals with $\epsilon(i) = (x_i, y_i)$ being the UAV's position at time i, P_{max} is the maximum transmit power possible from the transmitter, and v_{max} is the maximum speed of the UAV. The constraint (23) assures that the transmit power does not exceed the maximum possible for the transmitter device, and the constraint (24) limits the speed of UAV movement to its maximum possible for its rotors.

The MTRI formulation does not consider the energy cost of UAV movement. Therefore, we propose an alternative approach that aims to minimize the movement of the UAV while ensuring that the received light intensity does not fall below a pre-determined threshold, as follows:

MEMI : Minimum Energy With Minimum Intensity

$$\min_{\hat{\boldsymbol{\epsilon}}} \sum_{t=1}^{n-1} |\epsilon(t+1) - \epsilon(t)| \tag{25}$$

such that

$$I_r(t) \geq I_{min}, \quad t \in \{1, .., n\}. \tag{26}$$

(23), and (24),

where I_{min} is the minimum light intensity at the receiver that must be guaranteed throughout the time intervals being considered.

The difficulty with the MEMI formulation is its requirement for a pre-determined minimum light intensity, I_{min}. Determining the optimal I_{min} can be impractical, as setting it too high may render the optimization infeasible. To mitigate this challenge, conducting a priori field tests becomes necessary. Consequently, we propose another trajectory optimization problem, which takes into account the efficiency of movement in achieving better received light intensity, as follows:

MME : Maximum Movement Efficiency

$$\max_{\hat{\boldsymbol{\epsilon}}} \sum_{t=1}^{n-1} \frac{I_r(t+1)}{1 + |\epsilon(t+1) - \epsilon(t)|} \tag{27}$$

such that

(23) and (24).

B. Problem Solutions

For solving the UAV movement optimization problems in (22), (25), and (27), we adopted a time-ordered graph-based approach, illustrated in Figure 7. In this approach, we designate the source of the graph as the initial position of the UAV at

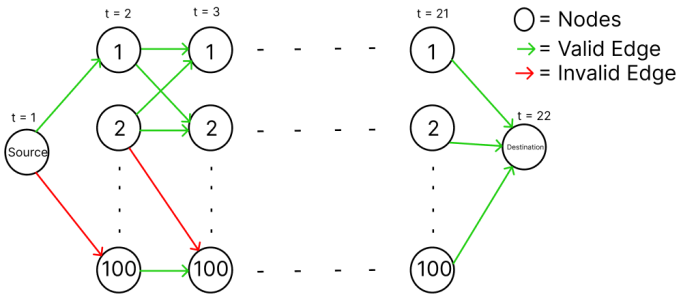

Fig. 7. Formation of Time-Ordered Graph.

$t = 1$. For each subsequent time instance ($t = 2$ to $t = n$), we consider the 100 possible coordinates as UAV positions, treating them as nodes or vertices for each layer of the graph. A destination node is assumed at the last layer after time instance $t = n$, with edges between the destination node and the nodes of the last layer ($t = n$) having zero weight. This design allows us to employ both shortest and longest path algorithms to find the trajectory between the source and destination, optimizing either to minimize or maximize the respective edge weights. This optimization spans from time instance $t = 1$ to $t = n$. Furthermore, edges are only connected between nodes of consecutive time instances, ensuring that the graph remains directed and acyclic. Each edge added to the graph represents the parameter being maximized or minimized for the respective optimization, as described in detail below.

1) MTRI: For the graph in MTRI, when there is an edge to be added between, for example, node u at time t and node v at time $t + 1$, it must pass the check to ensure that the distance between them is less than 1.57 meters. This maximum allowable distance is derived from the assumption that the maximum velocity (v_{max}) of the UAV is 1.57 m/s, and the time granularity (Δt) is 1 second. Additionally, this distance ensures that the UAV can reach all 8 adjacent nodes within one time step: 2 horizontally, 2 vertically, and 4 diagonally. Once this requirement is satisfied, the received light intensity of destination node v is set as the weight of the edge. Therefore, the weight of the directed edge $(u \rightarrow v)$ between them would be the received intensity $I_r(t + 1)$ associated with destination node v.

As stated in the problem formulation of MTRI, we aim to find the trajectory of the UAV that maximizes the summation of intensity across all time instances starting from $t = 1$. Since we have attributed the intensity of destination nodes as the edge weight in this directed acyclic graph, applying the longest path algorithm that utilizes topological sorting and dynamic programming will give us the trajectory with the highest summation of intensity in the form of the longest path. As described in Algorithm 1, two dictionaries are initialized for distance and path. The distance dictionary signifies the gained intensity in that trajectory and holds the maximum total intensity from the starting point to each vertex, initialized to negative infinity for all vertices. The path dictionary holds the longest path from the starting point to each vertex and is initialized to an empty list for all vertices.

Algorithm 1: Longest Path Algorithm

Function *Longest_Path_DAG(G)*:
  $top\_order \leftarrow$ **list of nodes in graph** G **in topological order**
  Initialize $dist$ **and** $paths$ **for all nodes in** G **as** $-\infty$ **and empty list respectively**
  $dist[top\_order[0]] \leftarrow 0$
  $paths[top\_order[0]] \leftarrow [top\_order[0]]$
  for *each node in* top_order **do**
    for *each* adj_node *in* $G.adj[node]$ **do**
      if $dist[node] + G[node][adj\_node]['weight'] > dist[adj\_node]$ **then**
        Update $dist[adj\_node]$ **with** $dist[node] + G[node][adj\_node]['weight']$
  $longest\_path\_length \leftarrow$ **maximum value in** $dist$
  $node\_with\_longest\_path \leftarrow$ **node with maximum value in** $dist$
  $longest\_path \leftarrow paths[node\_with\_longest\_path]$
  return $longest\_path$

The algorithm begins by performing a topological sort on the graph. Topological sort is a linear ordering of vertices such that if there is a node u at time t and a node v at time $t + 1$, vertex u precedes v in the ordering. The intensity gained from the starting point to itself is initialized to 0. The algorithm then processes the vertices in topological order. For each vertex, it updates the total intensity and path information. If the total intensity from the starting point to the current vertex, plus the weight of the edge to an adjacent vertex, exceeds the current total intensity to that adjacent vertex, the algorithm updates the intensity and path information accordingly. After processing all vertices, the final output from the path dictionary gives us the associated nodes along the optimized trajectory, which is the MTRI-optimized trajectory of the UAV for that particular starting position. We then proceed to apply the same algorithm to every possible starting position of the UAV, which amounts to 100 coordinates in this simulation. This process results in 100 uniquely optimized UAV trajectories.

2) MEMI: In the graph for MEMI, the nodes are added similarly to the MTRI, except there is an additional check while adding the edges, and the value of the edge weight is differently calculated, making this optimization a constrained shortest path problem. For there to be an edge between two nodes u of time t and v of time $t+1$, the node v must have an associated intensity value of I_{min} or higher, which in this case is 0.0003 mW/m^2 or higher. This value has been selected from the common range of the intensity heatmap as envisioned in the a-priori field test in Section V-A. The idea is that the value is not too high that the UAV does not get options to move, and also not too low

that the UAV does not need to move. The weight of the edge $(u \rightarrow v)$ is the distance between u and v.

Now, as we would like to minimize the summation of movement in terms of $|\epsilon(t+1) - \epsilon(t)|$, where $\epsilon(t)$ is the coordinate of u and $\epsilon(t+1)$ is the coordinate of v, and the edge weights are distances between nodes, which are non-negative. We can use Dijkstra's algorithm to find the shortest path from the source to the destination to perform the minimization. This will give us the shortest UAV trajectory while maintaining the minimum receiver intensity threshold I_{min} for every position of the UAV. Similar to the MTRI solution, we simulated 100 unique trajectories specific to 100 different starting positions of the UAV for this solution as well.

3) MME: In the graph for MME, the nodes and edges are added similarly to the MTRI, except the value of the edge weight is differently attributed. Now, as we would like to maximize the movement efficiency in terms of $\frac{I_r(t+1)}{1+|\epsilon(t+1)-\epsilon(t)|}$, if we set this term as the weight of the directed edge $(u \rightarrow v)$, we could use similar topological sorting and dynamic programming as shown in Algorithm 1 to find the longest path. This results in the optimized trajectory of the UAV that ensures maximum movement efficiency. Similar to the MTRI and MEMI solutions, we simulated 100 unique trajectories specific to 100 different starting positions of the UAV for this solution as well.

4) Time Complexity: For the MTRI and MME solutions, the overall time complexity of the function is $O(V+E)$, where V represents the number of vertices (or nodes) and E represents the maximum number of edges possible in the graph being formed to solve the problems. Similarly, the MEMI solution has an overall time complexity of $O((V+E)\log V)$, as Dijkstra's algorithm dominates the complexity.

The value of V depends on the quantization granularity in time and space. V includes one source and one destination node, and the number of positions the UAV can go to multiplied by the number of time intervals. This can be expressed as $V = 2+n\pi(v_{max}/\Delta t)^2$. In a similar manner, E depends on the spatial movement granularity as well as time granularity of the setup. The UAV can move to 9 different positions (i.e., horizontal, vertical, and diagonal movements). Hence, each node of the graph for $t = i$ can have at most 9 directed links with the nodes for $t = i+1$. The source node (i.e., corresponding to the position where UAV starts) can also have at most 9 directed links with nodes for $t = 2$. The destination node, however, will have a directed link from all the $\pi(v_{max}/\Delta t)^2$ nodes for $t = n+1$. This yields $E = 9 + (n-1)\pi(v_{max}/\Delta t)^2 + \pi(v_{max}/\Delta t)^2$. Putting it all together, the time complexity is $O(n(v_{max}/\Delta t)^2)$ for MTRI and MME, and $O(n(v_{max}/\Delta t)^2 \log(n(v_{max}/\Delta t)^2))$ for MEMI. Considering that UAV's movement speed does not yield many movement options and is fewer than the time slots being consider (i.e., $v_{max}/\Delta t)^2 < n$, MEMI's time complexity can be rewritten as $O((v_{max}/\Delta t)^2 n \log n)$.

Overall, the time complexity of these methods is quite manageable, and they can be performed in real-time. For instance, in our setup, V has a value of 2,002 (1+20*100+1, representing 1 source node, 100 nodes for each of the 20 time instances, and 1 destination node), and E has a value of 17,209 (1*9+19*100*9+100*1, as each node has a maximum of 9 possible edges among adjacent nodes, and the destination node connects with all 100 adjacent nodes). Storing a graph of this size is entirely feasible in a typical drone.

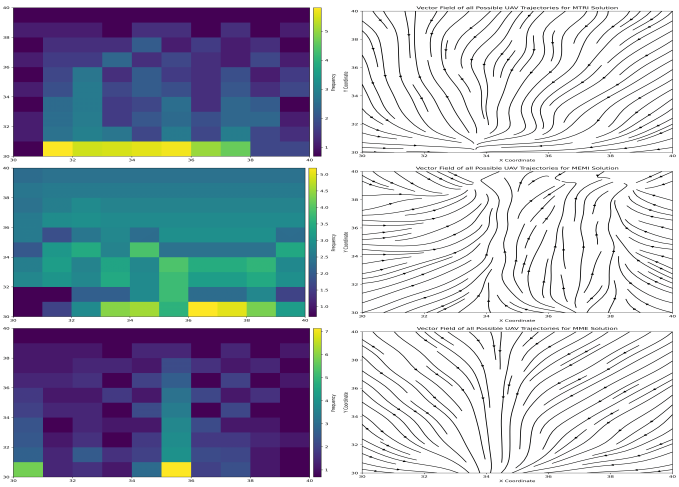

Fig. 8. UAV Trajectory for Deep Water.

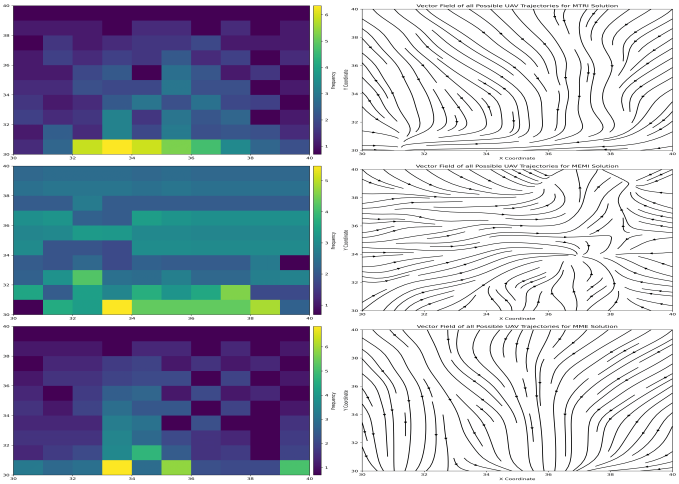

Fig. 9. UAV Trajectory for Intermediate Water.

VI. Simulation Results and Discussions

To understand if there exist general UAV trajectory patterns for optimizing the A2WOWC channel, we performed simulations. The assumptions for this simulation are consistent with those outlined in the subsection on assumptions (see Section III-A), along with the other parameters detailed in Table I. Two types of water body scenarios are considered here: high-peaked waves with higher steepness for intermediate water and low-peaked with lower steepness waves for deep water. Since there are 100 unique UAV starting positions, we computed optimized trajectories for each of them, resulting in a total of 100 trajectories for each of the three types of solution.

To illustrate the favorable UAV positions, we have adopted two approaches. Firstly, we generated a positional heatmap

portraying the total number of visits the UAV makes to each coordinate by combining data from all 100 different trajectories for 100 different starting positions. Secondly, utilizing the same data, we employed streamplots to represent the vector field of the UAV trajectories, depicting the UAV's propensity towards the most-visited favorable positions. As shown in Figure 8 and 9, both plots provide similar insights into the trajectories.

As mentioned previously, both MTRI and MME are solutions that primarily focus on achieving the maximum received intensity possible. However, the MME solution imposes a cost on UAV movement to maximize the value gained in terms of intensity over movement. In both deep and intermediate water scenarios, we observe that the UAV follows a similar trajectory pattern for MTRI and MME solutions. In contrast, with the MEMI solution, the optical transmitter must ensure a minimum intensity of 0.0003 mW/m^2 at the underwater receiver for every position along the UAV trajectory. This prerequisite leads to a more shifting movement for the MEMI solution, particularly in intermediate water scenarios due to the eccentric nature of the water surface compared to deep water.

VII. Conclusion

In summary, our research has extensively explored the realm of A2WOWC, with a specific emphasis on diverse air-water interfaces and their effect on the communication channel. Our findings underscore the viability of achieving optimal performance in visible light communication, even amidst the complexities of a dynamic water surface. This is made possible by implementing three meticulously optimized UAV movement strategies. The initial segment of our investigation demonstrated how variations in wave amplitude and horizontal shifts influence the end-to-end channel performance. Addressing the need for seamless communication across the ever-changing air-water interface, we proposed UAV movement optimization to adapt to these dynamic conditions. In the subsequent sections of our paper, we introduce three distinct movement optimization algorithms tailored for two different depths of water: intermediate and deep, focusing on performance, reliability, and value. Looking ahead, our future endeavors include incorporating more challenging medium parameters, such as scattering, turbulence, and random particles, into channel modeling, three-dimensional optical ray propagation, and UAV movements. We intend to develop sophisticated heuristics to effectively navigate these intricate conditions, further enhancing the robustness of A2WOWC systems.

References

[1] G. Benelli, A. Pozzebon, and M. Reaz, *RFID under water: Technical issues and applications*. InTech Rijeka, 2013.

[2] J. A. Catipovic, "Performance limitations in underwater acoustic telemetry," *IEEE Journal of Oceanic Engineering*, vol. 15, no. 3, pp. 205–216, 1990.

[3] Y. Chen, M. Kong, T. Ali, J. Wang, R. Sarwar, J. Han, C. Guo, B. Sun, N. Deng, and J. Xu, "26 m/5.5 gbps air-water optical wireless communication based on an ofdm-modulated 520-nm laser diode," *Optics express*, vol. 25, no. 13, pp. 14 760–14 765, 2017.

[4] G. Schirripa Spagnolo, L. Cozzella, and F. Leccese, "Underwater optical wireless communications: Overview," *Sensors*, vol. 20, no. 8, p. 2261, 2020.

[5] C. Shen, Y. Guo, X. Sun, G. Liu, K.-T. Ho, T. K. Ng, M.-S. Alouini, and B. S. Ooi, "Going beyond 10-meter, gbit/s underwater optical wireless communication links based on visible lasers," in *2017 opto-electronics and communications conference (OECC) and photonics global conference (PGC)*. IEEE, 2017, pp. 1–3.

[6] M. V. Jamali, A. Mirani, A. Parsay, B. Abolhassani, P. Nabavi, A. Chizari, P. Khorramshahi, S. Abdollahramezani, and J. A. Salehi, "Statistical studies of fading in underwater wireless optical channels in the presence of air bubble, temperature, and salinity random variations," *IEEE Transactions on Communications*, vol. 66, no. 10, pp. 4706–4723, 2018.

[7] Y. Baykal, "Higher order mode laser beam scintillations in oceanic medium," *Waves in Random and Complex media*, vol. 26, no. 1, pp. 21–29, 2016.

[8] H. M. Oubei, J. R. Duran, B. Janjua, H.-Y. Wang, C.-T. Tsai, Y.-C. Chi, T. K. Ng, H.-C. Kuo, J.-H. He, M.-S. Alouini *et al.*, "4.8 gbit/s 16-qam-ofdm transmission based on compact 450-nm laser for underwater wireless optical communication," *Optics express*, vol. 23, no. 18, pp. 23 302–23 309, 2015.

[9] M. S. Islam, M. Younis, and F.-S. Choa, "Optimizing acoustic signal quality for linear optoacoustic communication," in *ICC 2021-IEEE International Conference on Communications*. IEEE, 2021, pp. 1–6.

[10] A. S. Mohammed, S. A. Adnan, M. A. A. Ali, and W. K. Al-Azzawi, "Underwater wireless optical communications links: perspectives, challenges and recent trends," *Journal of Optical Communications*, no. 0, 2022.

[11] P. Land and A. K. Majumdar, "Demonstration of adaptive optics for mitigating laser propagation through a random air-water interface," in *Ocean Sensing and Monitoring VIII*, vol. 9827. SPIE, 2016, pp. 14–21.

[12] F. Blackmon and L. Antonelli, "Remote, aerial, trans-layer, linear and non-linear downlink underwater acoustic communication," in *OCEANS 2006*. IEEE, 2006, pp. 1–7.

[13] X. Cheng, H. Zheng, and C. Yan, "Ber evaluation and waveform analysis of nonlinear opto-acoustic communication system," *Optik*, vol. 124, no. 15, pp. 2000–2003, 2013.

[14] F. Tonolini and F. Adib, "Networking across boundaries: enabling wireless communication through the water-air interface," in *Proceedings of the 2018 Conference of the ACM Special Interest Group on Data Communication*, 2018, pp. 117–131.

[15] P. Nabavi and M. Yuksel, "Performance analysis of air-to-water optical wireless communication using spads," in *2019 IEEE Global Communications Conference (GLOBECOM)*. IEEE, 2019, pp. 1–6.

[16] C. Yang and F. Yang, "Communication interruption analysis for air-water wireless optical communication," in *2023 International Wireless Communications and Mobile Computing (IWCMC)*. IEEE, 2023, pp. 1022–1027.

[17] Q. Peng, G. Chen, X. Li, Q. Liao, and Y. Guo, "Performance improvement of underwater continuous-variable quantum key distribution via photon subtraction," *Entropy*, vol. 21, no. 10, p. 1011, 2019.

[18] S. De, "Contributions to the theory of stokes waves," in *Mathematical Proceedings of the Cambridge Philosophical Society*, vol. 51, no. 4. Cambridge University Press, 1955, pp. 713–736.

[19] M. S. Islam, M. Younis, and A. Ahmed, "Communication through air water interface using multiple light sources," in *2018 IEEE International Conference on Communications (ICC)*. IEEE, 2018, pp. 1–6.

[20] S. C. Shen, C. Y. Kuo, and M.-C. Fang, "Design and analysis of an underwater white led fish-attracting lamp and its light propagation," *International Journal of advanced robotic systems*, vol. 10, no. 3, p. 183, 2013.

[21] D. H. Goldstein, *Polarized light*. CRC press, 2017.

[22] G. Lérondel and R. Romestain, "Fresnel coefficients of a rough interface," *Applied Physics Letters*, vol. 74, no. 19, pp. 2740–2742, 1999.

[23] F. R. Tangherlini, "On snell's law and the gravitational deflection of light," *American Journal of Physics*, vol. 36, no. 11, pp. 1001–1004, 1968.

[24] M. Perlin, W. Choi, and Z. Tian, "Breaking waves in deep and intermediate waters," *Annual review of fluid mechanics*, vol. 45, pp. 115–145, 2013.